

Dynamic Constraint Based Energy Saving Control of Pneumatic Servo Systems

Khalid A. Al-Dakkan
Eric J. Barth
Michael Goldfarb

Department of Mechanical Engineering
Vanderbilt University
Nashville, TN 37235

Submitted to the *ASME Journal of Dynamic Systems, Measurement, and Control*

Version: August 7, 2003

Abstract

This paper proposes a control approach that provides significant energy savings for the control of pneumatic servo systems. The control methodology is formulated by decoupling the standard four-way spool valve used for pneumatic servo control into two three-way valves, then using the resulting two control degrees of freedom to simultaneously satisfy a performance constraint based on the sliding mode sliding condition, and an energy-saving dynamic constraint that minimizes cylinder pressures. The control formulation is presented, followed by experimental results that indicate significant energetic savings with essentially no compromise in tracking performance relative to a standard sliding mode approach. Relative to a standard four-way spool valve controlled pneumatic servo actuator under sliding mode control, the experimental results indicate energy savings of 27 to 45%, depending on the desired tracking frequency.

1 Introduction

A typical pneumatic servo system, which consists primarily of a proportionally controllable four-way spool valve and a pneumatic cylinder, is depicted in Fig. 1. In this system, the position of the valve spool controls the airflow into and out of each side of the cylinder, which in turn results in a pressure differential across the piston and thus imposes a force on the load. In such a system, feedback control is incorporated to command a valve spool motion that will result in a desired motion of the piston load. A considerable amount of work has been conducted in the modeling and feedback control of such systems, including the work by Shearer [1, 2, 3], Mannetje [4], Ben-Dov and Salcudean [5], Wang et al. [6], Maeda et al. [7], Ning and Bone [8], Bobrow and McDonell [9], and Richer and Hurmuzlu [10, 11], among others. Despite this prior work on the control of pneumatic servo systems, relatively little work has focused on the energetic efficiency of such systems. This topic has presumably received little attention from the research community because most applications draw energy from an essentially limitless reservoir of power (i.e., from a power plant). In many applications, however, the available energy is considerably more limited (e.g., in the case of a mobile robot), and in such cases, the energetic efficiency of the controller is significant. Fluid powered systems in particular offer intriguing possibilities with regard to the energetic efficiency of control. Specifically, the energetic role of an actuator at any given point in time is either to generate or dissipate power. In a fluid powered system, the energetic role of power dissipation can be provided passively by controlling the resistance to fluid flow. Therefore, ideally, a fluid powered system need only draw energy from the (high pressure) fluid supply when the actuator is generating power, but need not use the supply when dissipating power. Control approaches related to this notion have been investigated by Sanville [12], Quaglia and Gestaldi [13, 14], Pu et al. [15], Wang et al. [16], Kawakami et al.

[17], Arinaga et al. [18], and Yao and Liu [19]. Specifically, Sanville utilized a secondary reservoir in an open-loop system to collect exhaust air rather than vent it to atmosphere, and then used the reservoir as an auxiliary low-pressure supply. Quaglia and Gestaldi proposed a non-conventional pneumatic cylinder that incorporates multiple cylinder chambers embedded into a single actuator with the intent of recycling compressed air. Pu et al. describe a pneumatic arrangement that incorporates a standard four-way spool valve controlled pneumatic servoactuator, with an additional two-way valve between the two sides of the cylinder. They demonstrated “preliminary” results, but since no experimental comparisons were presented, it is unclear what improvements in efficiency were achieved. Wang et al. studied the use of input shaping to choose a command profile for point-to-point motions that would result in energy savings for closed loop pneumatic servoactuators, and showed that some velocity profiles could reduce energy demand relative to other profiles. Kawakami et al. and Arinaga et al. utilized metering circuits to reduce the airflow requirements for open-loop point-to-point motions. Finally, Yao and Liu used a combination of five two-way proportional valves in a hydraulic system in order to control the flow efficiently. Due to the absence of thermodynamic compressibility in the valves (i.e., choked and unchoked flow) and cylinder in hydraulic systems, however, the determination of the dynamic regime in which the (hydraulic) system can passively impose force is trivial, and thus the switching conditions are fairly simple and not of use for pneumatic systems. Further, no experimental comparisons to evaluate the efficiency of the proposed design were presented. Research focused on energetically efficient closed-loop control of a standard pneumatic servoactuator is conspicuously absent from the prior literature. This paper attempts to fill this void by introducing a control methodology that enables significant energetic savings in closed-loop controlled pneumatic servoactuation.

2 Control Approach

The proposed control approach is based on a standard sliding mode control approach, in which the single control degree of freedom (i.e., the spool position of the four-way valve) is utilized to satisfy what is commonly known as the sliding condition, which in turn provides stable tracking with a desired error dynamic (e.g., see [11]). In order to address an energy saving objective, the single four-way spool valve utilized in the standard configuration is decoupled into two three-way valves, as shown in Fig. 2, hence decoupling the discharging of one side of the cylinder from the charging of the opposite side. As such, the single actuation degree of freedom is influenced by two control degrees of freedom (i.e., the modified servoactuator is a two-input, single-output system). In the proposed energy-saving control approach, this additional degree of freedom is utilized to minimize the average cylinder pressure in addition to satisfying the sliding condition, which in turn minimizes the airflow utilized to track a desired trajectory. The net effect is a controller that only maintains the necessary output impedance required to track a given command. Specifically, standard sliding mode controllers provide good tracking performance, but in doing so consistently maintain a high actuator output impedance, regardless of the tracking demands. The proposed approach provides only the actuator output impedance required to achieve a desired tracking performance. As such, the output impedance of the proposed approach, and thus the required airflow, is significantly lower than that of the standard sliding mode control approach when the tracking demands are low. As the tracking demands increase, the output impedance (and thus the required airflow) of the proposed approach increases, until at high tracking demands (i.e., as the actuator approach power limits), the output impedance and energetic characteristics of the proposed method begin to approach that of standard sliding mode control, and the two approaches become in essence indistinguishable.

3 Modeling the Pneumatic Servo System

The texts [20, 21] describe variations on modeling pneumatic servoactuators. The model used in the work presented herein is reasonably standard, and is presented briefly here so that the model-based control approach can be described. The load dynamics of the system shown in Fig. 1 can be written as:

$$M\ddot{x} + B\dot{x} = P_a A_a - P_b A_b - P_{atm} A_r \quad (1)$$

where M is the payload plus the piston and rod assembly mass, B is the viscous friction coefficient, P_a and P_b are the absolute pressures in chambers a and b , respectively, P_{atm} is atmospheric pressure, A_a and A_b are the effective areas of each side of the piston, and A_r is the cross-sectional area of the piston rod. Note that for the work presented here, the Coulomb friction forces from the piston and rod seals were considered disturbances. It should be noted, however, that the proposed approach does not require this assumption, and as such, the piston and rod seal friction could be explicitly model if so desired. Assuming air is a perfect gas undergoing an isothermal process, the rate of change of the pressure inside each chamber of the cylinder can be expressed as:

$$\dot{P}_{(a,b)} = \frac{RT}{V_{(a,b)}} \dot{m}_{(a,b)} - \frac{P_{(a,b)}}{V_{(a,b)}} \dot{V}_{(a,b)} \quad (2)$$

where $P_{(a,b)}$ is the pressure inside each side of the cylinder, $\dot{m}_{(a,b)}$ is the mass flow rates into or out of each side of the cylinder, R is the universal gas constant, T is the fluid temperature, and $V_{(a,b)}$ is the volume of each cylinder chamber. The volume in each chamber, and the volume rate of change, is related to the rod position x by:

$$V_a = V_{mid,a} + A_a x \quad (3)$$

$$V_b = V_{mid,b} - A_b x \quad (4)$$

$$\dot{V}_a = A_a \dot{x} \quad (5)$$

$$\dot{V}_b = -A_b \dot{x} \quad (6)$$

where $V_{mid,a}$ and $V_{mid,b}$ are the volumes of chambers a and b respectively at $x = 0$. Note that if the process were assumed adiabatic rather than isothermal (i.e., at the other extreme of the heat transfer assumption), the right-hand-side of Eq. (2) would be multiplied by the ratio of specific heats (approximately 1.4 for air), but the pressure dynamics would otherwise remain the same (see [10] for details). As such, as long as the control approach is robust to limited parameter variation, the control problem is not sensitive to assumptions regarding the presence of heat transfer. Based on isentropic flow assumptions, the mass flow rate through a valve orifice with *effective* area A_v for a compressible substance can be stated functionally as:

$$\dot{m}_a = A_{v,a} \Psi_a = \begin{cases} A_{v,a} \Psi_a(P_s, P_a) & \text{for } A_{v,a} \geq 0 \text{ (charge)} \\ A_{v,a} \Psi_a(P_a, P_{atm}) & \text{for } A_{v,a} < 0 \text{ (discharge)} \end{cases} \quad (7)$$

$$\dot{m}_b = A_{v,b} \Psi_b = \begin{cases} A_{v,b} \Psi_b(P_s, P_b) & \text{for } A_{v,b} \geq 0 \text{ (charge)} \\ A_{v,b} \Psi_b(P_b, P_{atm}) & \text{for } A_{v,b} < 0 \text{ (discharge)} \end{cases} \quad (8)$$

where the normalized mass flow rate $\Psi_{(a,b)}$ will reside in either a sonic (choked) or subsonic (unchoked) flow regime:

$$\Psi(P_u, P_d) = \begin{cases} \frac{C_1 C_f P_u}{\sqrt{T}} & \text{if } \frac{P_d}{P_u} \leq C_r \text{ (choked)} \\ \frac{C_2 C_f P_u}{\sqrt{T}} \left(\frac{P_d}{P_u}\right)^{1/k} \sqrt{1 - \left(\frac{P_d}{P_u}\right)^{(k-1)/k}} & \text{otherwise (unchoked)} \end{cases} \quad (9)$$

where C_f is the discharge coefficient of the valve, P_u and P_d are the upstream and downstream pressures, respectively, T is the air temperature (which given the isothermal assumption is con-

stant), k is the ratio of specific heats, C_r is the pressure ratio that divides the flow regimes into unchoked and choked flow, and C_1 and C_2 are constants defined as:

$$C_1 = \sqrt{\frac{k}{R} \left(\frac{2}{k+1}\right)^{(k+1)/(k-1)}} \quad (10)$$

and

$$C_2 = \sqrt{\frac{2k}{R(k-1)}} \quad (11)$$

The effective (signed) valve areas $A_{v,a}$ and $A_{v,b}$ can be assigned according to the positive and negative displacement of the spool of each valve, y_a and y_b respectively, and the area uncovered geometrically by the spool:

$$A_{v,(a,b)} = f(|y_{(a,b)}|) \text{sgn}(y_{(a,b)}) \quad (12)$$

where $f(\cdot)$ is the orifice area uncovered by the spool, the exact form of which depends on the spool and orifice geometry.

4 Standard Sliding Mode Control of a Pneumatic Servoactuator

In the control of a standard pneumatic servo system, a four-way spool valve (as shown in Fig. 1) is used to connect one cylinder chamber to the pressure supply, while the other will be connected to atmosphere, both with the same effective area. As such, the effective valve area command A_v for the four-way spool valve can be defined as follows:

$$A_v = A_{v,a} = -A_{v,b} \quad (13)$$

Specifically, a positive valve area command corresponds to charging chamber a and discharging b , while a negative valve area command corresponds to the opposite. Given these definitions, combined with the system behavior described by Eqs. (1-12), the system dynamics for a positive control valve command (charging a and discharging b) are described by:

$$M\ddot{x}^{(3)} + B\ddot{x} = RTA_v \left(\frac{A_a}{V_a} \Psi(P_s, P_a) + \frac{A_b}{V_b} \Psi(P_b, P_{atm}) \right) - \left(\frac{P_a A_a \dot{V}_a}{V_a} - \frac{P_b A_b \dot{V}_b}{V_b} \right) \quad (14)$$

and the system dynamics for a negative control valve command (charging b and discharging a) are described by:

$$M\ddot{x}^{(3)} + B\ddot{x} = RTA_v \left(\frac{A_a}{V_a} \Psi(P_a, P_{atm}) + \frac{A_b}{V_b} \Psi(P_s, P_b) \right) - \left(\frac{P_a A_a \dot{V}_a}{V_a} - \frac{P_b A_b \dot{V}_b}{V_b} \right) \quad (15)$$

Due to the extensive nonlinearities (as described by Eqs. (9-15)) and to the presence of parametric uncertainty in pneumatic systems, sliding mode control is generally well suited to the control of pneumatic servoactuators. For the system shown in Fig.1, the plant output, which is the load position x , must be differentiated three times to produce the control input, which is the valve area A_v , and as such the system is characterized by third order dynamics. Defining a sliding surface as:

$$s = \left(\frac{d}{dt} + \lambda \right)^{(n-1)} e \quad (16)$$

where e is the tracking error of the piston position x compared to the desired piston position x_d (i.e., $e = x - x_d$), λ is a strictly positive constant, and n is the number of times the output must be differentiated to recover the input (which as previously described for this system is three). In standard sliding mode control, the controller consists of two components, an equivalent control law, which utilizes model and error information to provide marginal stability in the sense of Lyapunov, and a switching component, which robustly enforces the condition $\dot{V} < 0$ (where V is the Lyapunov function), and thus provides for uniform asymptotic stability. Thus the form of sliding mode control is given by:

$$A_v = A_{v,eq} - K \text{sat}\left(\frac{s}{\Phi}\right) \quad (17)$$

where K is a strictly positive gain, Φ is the boundary layer thickness, and $A_{v,eq}$ is the equivalent control component of the valve area command. The equivalent control component of Eq. (17) is formulated by forcing $\dot{s} = 0$, which for this system yields:

$$x^{(3)} = x_d^{(3)} - 2\lambda(\ddot{x} - \ddot{x}_d) - \lambda^2(\dot{x} - \dot{x}_d) \quad (18)$$

Combining Eq. (18) with the system dynamics described by Eqs. (9-15) yields the equivalent control term for standard sliding mode control:

$$A_{v,eq} = \begin{cases} \frac{M(x_d^{(3)} - 2\lambda(\ddot{x} - \ddot{x}_d) - \lambda^2(\dot{x} - \dot{x}_d)) + B\ddot{x} + (\frac{P_a A_a \dot{V}_a}{V_a} - \frac{P_b A_b \dot{V}_b}{V_b})}{RT \left(\frac{A_a}{V_a} \Psi(P_s, P_a) + \frac{A_b}{V_b} \Psi(P_b, P_{atm}) \right)} & \text{for } A_v \geq 0 \\ \frac{M(x_d^{(3)} - 2\lambda(\ddot{x} - \ddot{x}_d) - \lambda^2(\dot{x} - \dot{x}_d)) + B\ddot{x} + (\frac{P_a A_a \dot{V}_a}{V_a} - \frac{P_b A_b \dot{V}_b}{V_b})}{RT \left(\frac{A_a}{V_a} \Psi(P_a, P_{atm}) + \frac{A_b}{V_b} \Psi(P_s, P_b) \right)} & \text{otherwise.} \end{cases} \quad (19)$$

The switching condition of Eq. (19) simply indicates that the controller should use the equivalent control law corresponding to the proper direction of control effort. That is, if the sign of A_v is positive, then according to Eq. (13), the system will be charging chamber a and discharging b , and as such the equivalent control corresponding to the dynamics of that case should be utilized in computing the control effort. If the sign of A_v is negative, the system will be charging chamber b and discharging a , and so the corresponding equivalent control should be used.

5 Dynamic Constraint Based Energy Saving Sliding Mode Control

As previously described, decoupling the single four-way spool valve into two three-way valves, as shown in Fig. 2, provides the single actuation degree of freedom with two control degrees of freedom (i.e., provides a two-input, single-output system). Practically speaking, this amounts to

replacing the fixed relationship between the valve areas imposed by the four-way spool valve in Eq. (13) with a state dependent relationship. In the proposed energy-saving control approach, this additional degree of freedom is utilized to minimize the pressures in the actuator in addition to satisfying the sliding condition, which in turn minimizes the airflow utilized to track the desired trajectory. Specifically, the control law is derived by combining the standard sliding mode control sliding condition objective together with an energy saving objective. The energy in a pneumatic pressure supply (i.e., in a tank) is proportional to the mass in that tank, assuming an ideal gas at some temperature. Thus, the objective of minimizing the energy utilized is equivalent to minimizing the mass flow rate. For a given fixed volume (i.e., the cylinder actuator) and at a given temperature, the pressure in the cylinder is proportional to the mass in that cylinder. Therefore, the objective of minimizing the energy utilized from the pressure source is equivalent to minimizing the pressure in each cylinder chamber. Accordingly, a positive definite objective function can be defined as,

$$J = \frac{1}{2} P_a^2 + \frac{1}{2} P_b^2 \quad (20)$$

the minimization of which will result in a minimum usage of source energy. Likewise, the reduction of this objective function will result in the reduction of source energy used. A first order dynamic that drives the objective function to some target value can be constructed as:

$$\dot{J} = -\eta(J - J_{\text{target}}) \quad (21)$$

where J_{target} is the desired squared mean average pressure in the absence of tracking demands, and η is a strictly positive constant that determines the rate of convergence of the dynamic constraint of Eq. (21). In this work, $J_{\text{target}} = J(P_{\text{atm}}, P_{\text{atm}})$, which implies that in the absence of tracking demands, the pressure in each chamber of the cylinder will converge to atmospheric (since it

cannot be driven below atmospheric). The requisite mass flow rate for valve b (which is proportional to the commanded effective valve area $A_{v,b}$) can be described by combining Eq. (21) with the definition of J and the system model given by Eqs. (1-11):

$$\dot{m}_b = \left(\frac{P_R}{V_R}\right) \frac{(\dot{V}_a - \frac{\eta}{2} V_a)}{RT} P_a + \frac{(\dot{V}_b - \frac{\eta}{2} V_b)}{RT} P_b - \left(\frac{P_R}{V_R}\right) \dot{m}_a + \frac{\eta V_b}{RT P_b} J_{\text{target}} \quad (22)$$

where P_R is chamber pressure ratio P_a/P_b , and V_R is chamber volume ratio V_a/V_b . Therefore, the static relation of a four-way spool valve imposed by Eq. (13) has been replaced by a state dependent relationship of the form:

$$A_{v,b} \Psi_b = -\left(\frac{P_R}{V_R}\right) A_{v,a} \Psi_a + g(P_a, P_b, x, \dot{x}, J_{\text{target}}) \quad (23)$$

In formulating the control law, the requisite mass flow rate for valve a is obtained by differentiating Eq. (1) and using the expression of the rate of change of the pressure inside the chambers described by Eq. (2), which yields:

$$x^{(3)} = \frac{A_a RT}{MV_a} \dot{m}_a - \frac{A_a P_a}{MV_a} \dot{V}_a - \frac{A_b RT}{MV_b} \dot{m}_b + \frac{A_b P_b}{MV_b} \dot{V}_b - \frac{b}{M} \ddot{x} \quad (24)$$

The desired mass flow rate of chamber a is then found by substituting Eq. (22) into Eq. (24), which gives:

$$\dot{m}_a = \frac{x^{(3)} + \frac{A_a \dot{V}_a}{MV_a} \left(1 + A_R^{-1} \left(1 - \frac{\eta V_a}{2 \dot{V}_a}\right)\right) - \frac{A_b \dot{V}_b}{MV_b} \left(1 + A_R^{-1} \left(1 - \frac{\eta V_b}{2 \dot{V}_b}\right)\right) P_b + \frac{b}{M} \ddot{x} + \frac{\eta A_b}{M P_b} J_{\text{target}}}{\frac{RT A_a}{MV_a} (1 + A_R^{-1} P_R)} \quad (25)$$

where A_R is the area ratio given by A_a/A_b , and Eq. (18) is used to enforce the equivalent control condition $\dot{s} = 0$ via the quantity $x^{(3)}$. Utilizing Eq. (9), (22), and (25), the equivalent control commands for each respective valve are:

$$A_{v,a,eq} = \begin{cases} \frac{\dot{m}_a}{\Psi(P_s, P_a)} & \text{for } A_{v,a} > 0 \text{ (charging chamber } a) \\ \frac{\dot{m}_a}{\Psi(P_a, P_{atm})} & \text{otherwise (discharging chamber } a) \end{cases} \quad (26)$$

$$A_{v,b,eq} = \begin{cases} \frac{\dot{m}_b}{\Psi(P_b, P_{atm})} & \text{for } A_{v,b} < 0 \text{ (discharging chamber } b) \\ \frac{\dot{m}_b}{\Psi(P_s, P_b)} & \text{otherwise (charging chamber } b) \end{cases} \quad (27)$$

where $A_{v,a,eq}$ and $A_{v,b,eq}$ are the equivalent valve area commands of the valves connected to chambers a and b , respectively. The complete (i.e., robust) control law is formed by adding a robustness component to each of the equivalent control laws, as described by Eq. (17).

6 Experiments

Experiments were conducted to compare the tracking performance and average required mass flow rate of the proposed dynamic constraint based control versus that of a standard sliding mode controller. A schematic for the system setup is illustrated in Fig. 2. The double acting cylinder (Bimba 314-DXP) used in the experiment has a stroke length of 10.2 cm (4.0 in), inner diameter of 5.1 cm (2.0 in), and piston rod diameter of 1.6 cm (0.62 in). Two four-way proportional valves (PositioneX SVP-360) are attached to the chambers with two ports of each valve blocked to make the valves function as three-way valves. A brass block serves as a mass load of 10 kg (22 lb), which slides on a track with linear bearings (Thompson 1CBO8FAOL10). Three pressure transducers (Omega PX202-200GV) are attached to the pressure supply tank and each cylinder chamber, respectively, and a linear potentiometer (Midori LP-100F) with 10 cm (3.94 in) maximum travel measures the linear position of the inertial load. Control is provided by a Pentium 4 computer with an A/D card (National Instruments PCI-6031E), which drives the two pro-

portional valves via a pair of KEPCO bipolar power supply/amplifiers. The control inputs are the valve areas, which are commanded indirectly by commanding the spool displacements.

Model parameters used for the model-based controller were $M=11.4$ kg (25 lbs), $B= 13.1$ kg/s (28.8 lb/s), $A_a=20.3$ cm² (3.14 in²), $A_b=18.2$ cm² (2.83 in²), $C_f=0.8$, $C_r=0.528$, $k=1.4$, $T=298$ K, and $R=287$ m²/(s²K). Note also that each chamber has a dead-space volume of 18 cm³ (0.8 in³), which is needed in relating each chamber volume to the measured piston position, and that the valve commands were saturated at the maximum valve openings $A_{v,max}=7.35$ mm² (0.0114 in²). These parameters were obtained via direct measurement when possible, or through calculation when experimental measurement was not possible.

The sliding mode control gains and boundary layer thicknesses used in the control experiments were selected based on the system model and desired tracking bandwidth, then tuned to provide good tracking performance, first via simulation and then by experiment. Improved performance for both approaches was achieved with variable robustness gains, where the gains were simply increased linearly with increased tracking error, such that:

$$K = k_{min} + k_{slope} |s| \quad (28)$$

Note that the absolute value operator ensures that K is always strictly positive (i.e., K always increases with the magnitude of the tracking error). Equation (28) was additionally saturated to limit the amount by which the gain could vary. Finally, note that the variable gain does not violate any sliding mode stability or performance robustness guarantees, since as formulated, it can be guaranteed to be both positive and greater than some minimum value, as required by the degree of model uncertainty. For the standard sliding mode controller, the control gains were selected as:

$$\begin{aligned}
\lambda &= 100 \text{ s}^{-1} \\
\Phi &= 38.5 \text{ m/s}^2 \text{ (1500 in/s}^2\text{)} \\
k_{min} &= 3.0 \text{ mm}^2 \text{ (0.0045 in}^2\text{)} \\
k_{slope} &= 0.0018 \text{ mm}^2\text{s (2.7x10}^{-6}\text{ in}^2\text{s)} \\
3.0 \text{ mm}^2 \text{ (0.0045 in}^2\text{)} &\leq K \leq 5.5 \text{ mm}^2 \text{ (0.0085 in}^2\text{)}
\end{aligned} \tag{29}$$

For the dynamic constraint based controller, the control gains were selected as:

$$\begin{aligned}
\lambda &= 620 \text{ s}^{-1} \\
\Phi &= 256 \text{ m/s}^2 \text{ (10,000 in/s}^2\text{)} \\
k_{min} &= 2.0 \text{ mm}^2 \text{ (0.003 in}^2\text{)} \\
k_{slope} &= 0.00022 \text{ mm}^2\text{s (3.3x10}^{-7}\text{ in}^2\text{s)} \\
2.0 \text{ mm}^2 \text{ (0.003 in}^2\text{)} &\leq K \leq 4.1 \text{ mm}^2 \text{ (0.0063 in}^2\text{)}
\end{aligned} \tag{30}$$

The energy saving dynamic constraint control parameters (i.e., parameters for Eq. (21)) were selected as:

$$\begin{aligned}
\eta &= 700 \text{ s}^{-1} \\
J_{target} &= 10,200 \text{ kPa}^2 \text{ (213 psia}^2\text{)}
\end{aligned} \tag{31}$$

Recall that J_{target} , as given by Eq. (20), results from choosing both desired chamber pressures as atmospheric.

For each experiment, the average mass flow rate was found by charging a 5-gallon pressure supply tank to approximately 600 kPag (90 psig) before running each experiment and measuring the tank pressure as the experiment was performed. Assuming the air in the supply tank to be an ideal gas undergoing an isothermal process, the energy in the fixed-volume tank is proportional to the mass, which is in turn proportional to the tank pressure. Tracking experiments were conducted for sinusoidal frequencies of 0.25 Hz through 1.5 Hz. The experimental results of tracking performance for 0.25 Hz sinusoidal command signal are shown in Figs. 3 and 4 for standard sliding mode control and dynamic constraint based control, respectively. Both systems

demonstrate similar tracking performance. Fig. 5 shows the supply tank pressure during the initial 30-second tracking history for the sinusoidal trajectories shown in Figs. 3 and 4, demonstrating clearly the energy savings provided by the dynamic constraint based approach. Fig. 6 shows the pressure variations in both chambers for standard control (the two high pressure traces) and dynamic constraint based control (the two low pressure traces). As indicated by the figure, the mean pressures in the dynamic constraint based control hover just above atmospheric pressure, yielding a low actuator output impedance. In fact, in the absence of tracking demands, the chamber pressures will converge to atmospheric (or whatever mean pressures correspond to J_{target}).

Figs. 7 and 8 show sinusoidal tracking of a 1.5 Hz sinusoid for standard sliding mode and dynamic constraint based control, respectively, demonstrating essentially the same tracking performance. Fig. 9 shows the supply tank pressure during the initial 30-second tracking history for the sinusoidal trajectories shown in Figs. 7 and 8, demonstrating clearly the energy savings. The flow rate savings observed during the 1.5 Hz tracking are less than those observed during the 0.5 Hz tracking, due to the fact that the actuator demands are greater for the higher frequency tracking, and thus the actuator output impedance must be higher to provide the desired degree of tracking performance. The increase in required actuator output impedance is reflected in the data shown in Fig. 10, which compared to Fig. 6, indicates noticeably higher average chamber pressures for the dynamic constraint based control case.

A summary of the average energy (i.e., mass flow rate) savings for various sinusoidal tracking frequencies is listed in Table 1. As illustrated in the table, the maximum energy savings occur at 0.5 Hz, somewhere between the lowest and highest tracking frequencies. This is due to the fact that at very low frequencies, the dynamics of the pneumatic servoactuator is largely in-

fluenced by Coulomb friction, which requires a high output impedance for accurate tracking performance. Large inertial forces at higher frequencies similarly require a high actuator output impedance, and thus diminish the energy savings. As shown in the table, the maximum energy savings for this system occurs at approximately 0.5 Hz, which lies somewhere between the two extremes of friction-influenced dynamics and high actuator demand.

7 Conclusion

This paper presents an energy savings approach to the control of pneumatic servoactuation systems. The control approach is in essence a variable impedance controller, which maintains only the output impedance required to track the desired trajectory, and thus minimizes the required mass flow rate of air. Experiments demonstrate that the power consumption of a pneumatic servo system is reduced by as much as 45%, with essentially no sacrifice in tracking performance. The maximum energy saving for the system tested occurs at a frequency of 0.5 Hz, which is somewhere between the friction domination of low frequency motion and the large actuator demands required to overcome inertial forces at higher frequencies.

References

- [1] Shearer, J. L., "Study of Pneumatic Processes in the Continuous Control of Motion with Compresses Air – I," *Transactions of the ASME*, vol. 78, pp. 233-242, 1956.
- [2] Shearer, J. L., "Study of Pneumatic Processes in the Continuous Control of Motion with Compresses Air – II," *Transactions of the ASME*, vol. 78, pp. 243-249, 1956.
- [3] Shearer, J. L., "Nonlinear Analog Study of a High-Pressure Servomechanism," *Transactions of the ASME*, vol. 79, pp. 465-472, 1957.
- [4] Mannetje, J. J., "Pneumatic Servo Design Method Improves System Bandwidth Twenty-fold," *Control Engineering*, vol. 28, no. 6, pp. 79-83, 1981.

- [5] Ben-Dov, D. and Salcudean, S. E., "A Force Controlled Pneumatic Actuator," *IEEE Transactions on Robotics and Automation*, vol. 14, no. 5, pp. 732-742, 1998.
- [6] Wang, J., Pu, J., and Moore, P., "A practical control strategy for servo-pneumatic actuator systems," *Control Engineering Practice*, vol. 7, pp. 1483-1488, 1999.
- [7] Maeda, S., Kawakami, Y., and Nakano, K., "Position Control of Pneumatic Lifters," *Transactions of Japan Hydraulic and Pneumatic Society*, vol. 30, no. 4, pp. 89-95, 1999.
- [8] Ning, S. and Bone, G. M., "High Steady-State Accuracy Pneumatic Servo Positioning System with PVA/PV Control and Friction Compensation," *Proceeding of the 2002 IEEE International Conference on Robotics & Automation*, pp. 2824-2829, 2002.
- [9] Bobrow, J., and McDonell, B., "Modeling, Identification, and Control of a Pneumatically Actuated, Force Controllable Robot," *IEEE Transactions on Robotics and Automation*, vol. 14, no. 5, pp. 732-742, 1998.
- [10] Richer, E. and Hurmuzlu, Y., "A High Performance Pneumatic Force Actuator System: Part I-Nonlinear Mathematical Model" *ASME Journal of Dynamic Systems, Measurement, and Control*, vol. 122, no. 3, pp. 416-425, 2000.
- [11] Richer, E. and Hurmuzlu, Y., "A High Performance Pneumatic Force Actuator System: Part II-Nonlinear Control Design" *ASME Journal of Dynamic Systems, Measurement, and Control*, vol. 122, no. 3, pp. 426-434, 2000.
- [12] Sanville, F. E., "Two-level Compressed Air Systems for Energy Saving," The 7th International Fluid Control Symposium, pp. 375-383, 1986.
- [13] Quaglia, G. and Gastaldi, L., "The Design of Pneumatic Actuator with Low Energy Consumption," The 4th Triennial International Symposium on Fluid Control, Fluid Measurement, and Visualization, pp. 1061-1066, 1994.
- [14] Quaglia, G. and Gastaldi, L., "Model and Dynamic of Energy Saving Pneumatic Actuator," The 4th Scandinavian International Conference on Fluid Power, vol. 1, 481-492, 1995.
- [15] Pu, J., Wang, J. H., Moore, P. R., and Wong, C. B., "A New Strategy for Closed-loop Control of Servo-Pneumatic Systems with Improved Energy Efficiency and System Response," The Fifth Scandinavian International Conference on Fluid Power, pp. 339-352, 1997.
- [16] Wang, J., Wang, J-D., Liao, V., "Energy Efficient Optimal Control of Pneumatic Actuator Systems," *Systems Science*, Vol. 26, 3, pp. 109-123, 2000.
- [17] Kawakami, Y., Terashima, Y., Kawai, S., "Application of Energy-saving to Pneumatic Driving Systems," Proc. 4th JHPS International Symposium, pp. 201-206, 1999.
- [18] Arinaga, T., Kawakami, Y., Terashima, Y., and Kawai, S., "Approach for Energy-Saving of Pneumatic Systems," Proceedings of the 1st FPNI-PhD Symposium, pp. 49-56, 2000.

- [19] Yao, B., and Liu, S., “Energy-Saving Control of Hydraulic Systems with Novel Programmable Valves,” Proc. 4th World Congress on Intelligent control and Automation, pp. 3219-3223, 2002.
- [20] Burrows, C. R., Fluid Power Servomechanisms, Butler & Tanner Ltd, London, 1972.
- [21] McCloy, D., and Martin, H., Control of Fluid Power, Ellis Horwood Limited, Chichester, England, 1980.

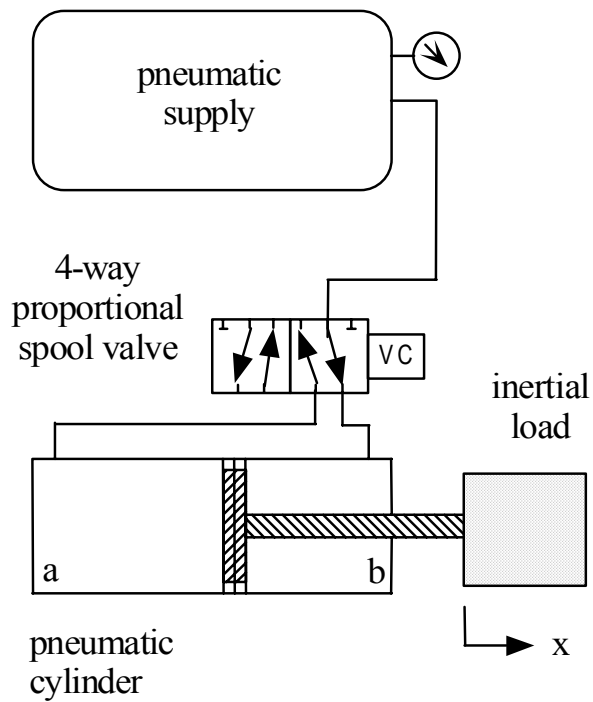


Fig. 1. A standard pneumatic servo actuator driving an inertial load.

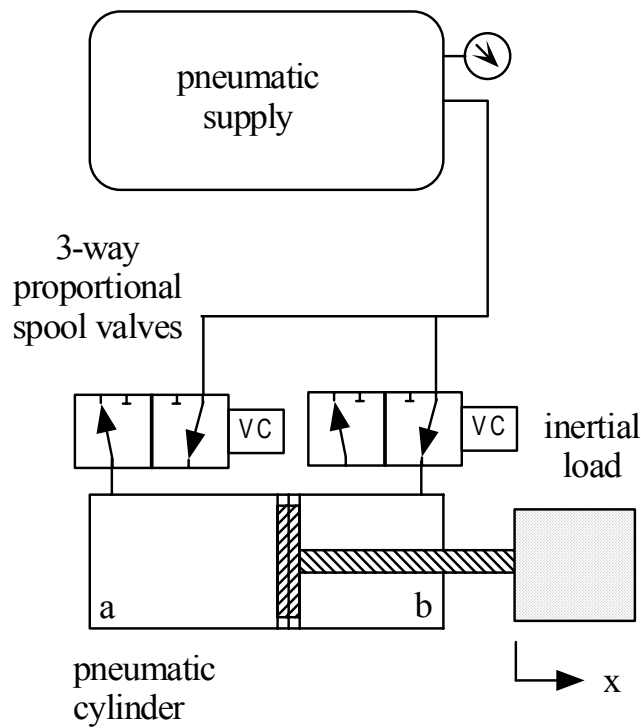


Fig. 2. Modification of standard pneumatic servo actuator for accommodating dynamic constraint based control architecture.

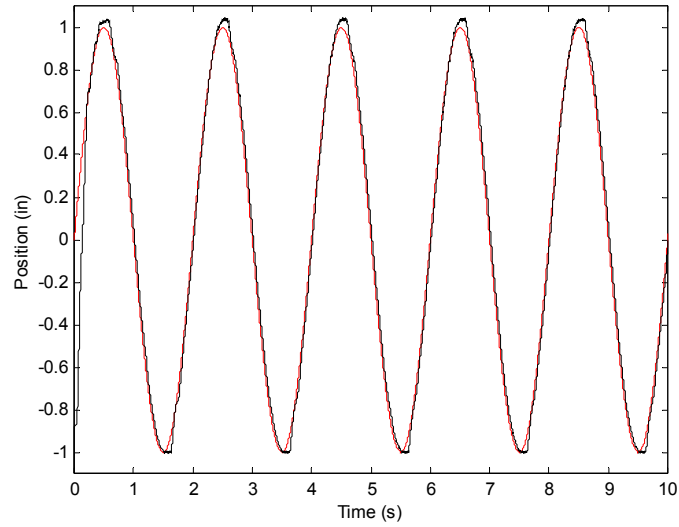


Fig. 3. Standard sliding mode control for 0.5 Hz sinusoidal tracking (black is actual position, gray is desired).

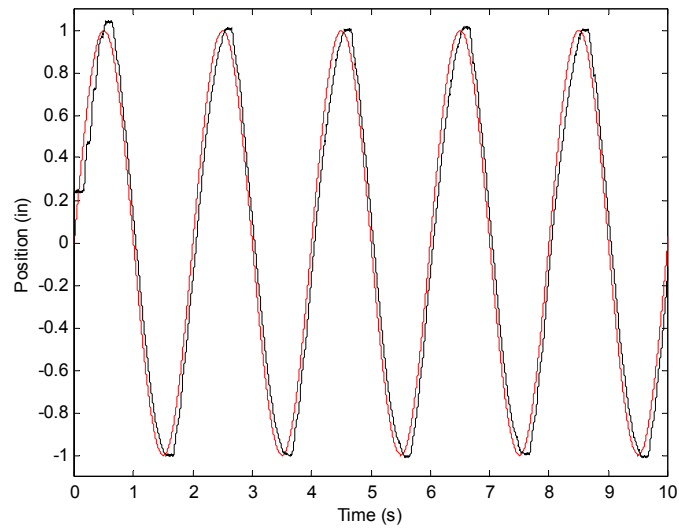


Fig. 4. Dynamic constraint based control for 0.5 Hz sinusoidal tracking (black is actual position, gray is desired).

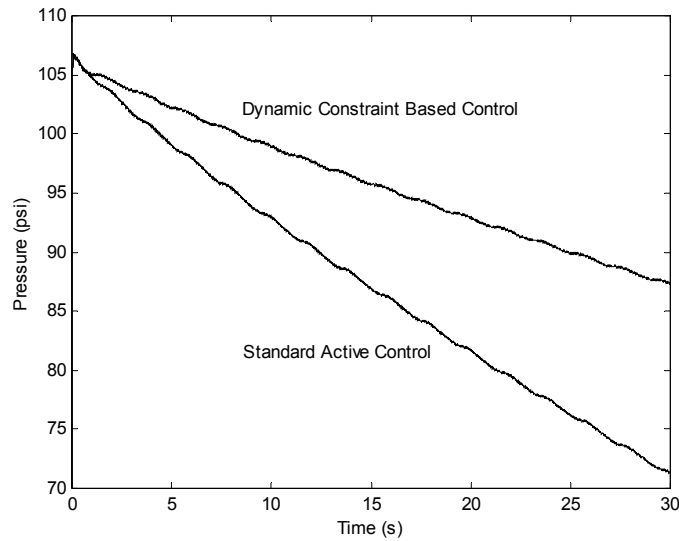


Fig. 5. Pressure drop in the supply tank over a 30-second interval during both dynamic constraint based control and standard control of 0.5 Hz sinusoidal tracking.

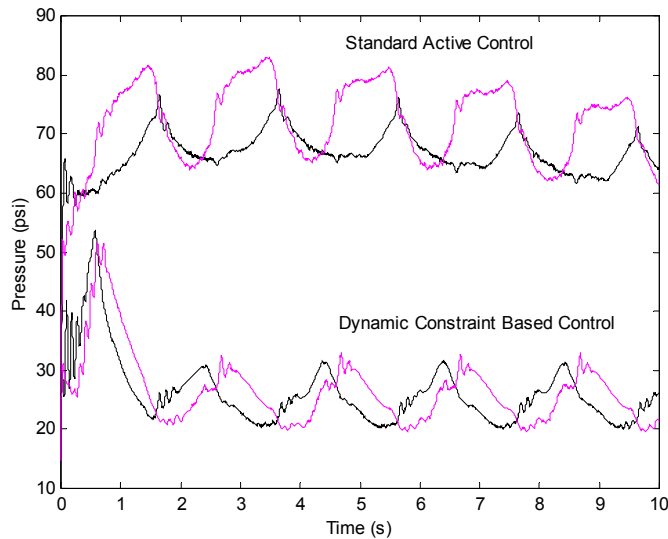


Fig. 6. Pressure variation in cylinder chambers for dynamic constraint based control versus standard sliding mode control for 0.5 Hz sinusoidal tracking (black is chamber *a* pressure, gray is chamber *b* pressure).

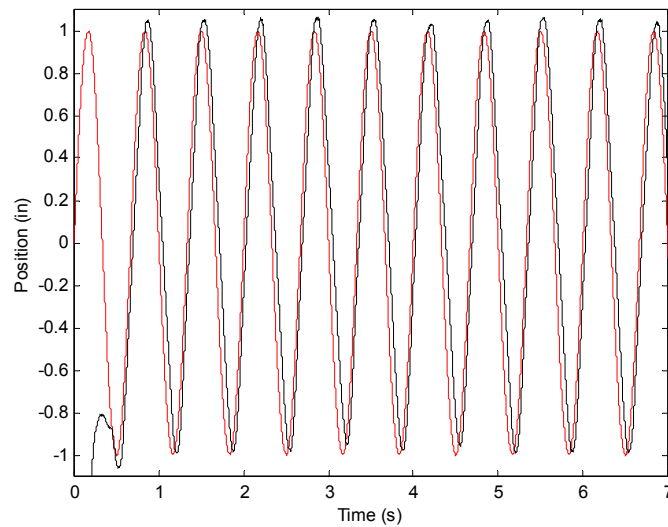


Fig. 7. Standard sliding mode control for 1.5 Hz sinusoidal tracking (black is actual position, gray is desired).

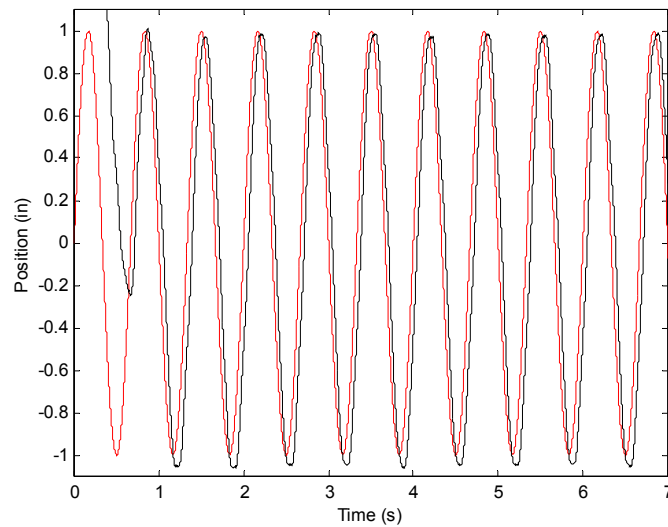


Fig. 8. Dynamic constraint based control for 1.5 Hz sinusoidal tracking (black is actual position, gray is desired).

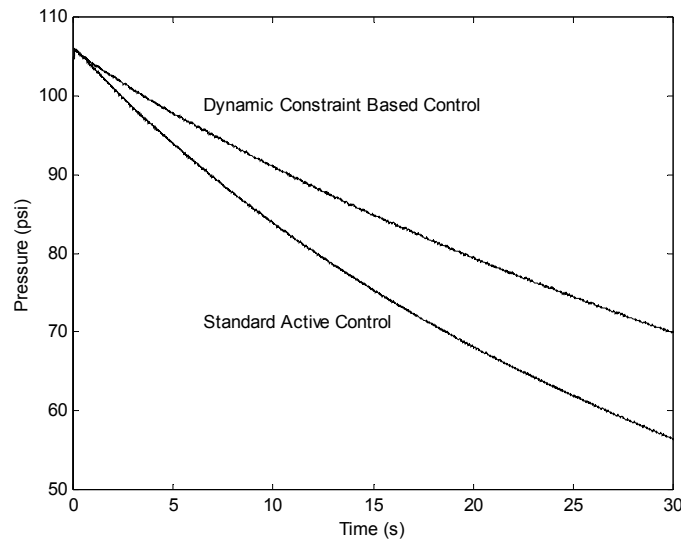


Fig. 9. Pressure drop in the supply tank over a 30-second interval during both dynamic constraint based control and standard sliding mode control of 1.5 Hz sinusoidal tracking.

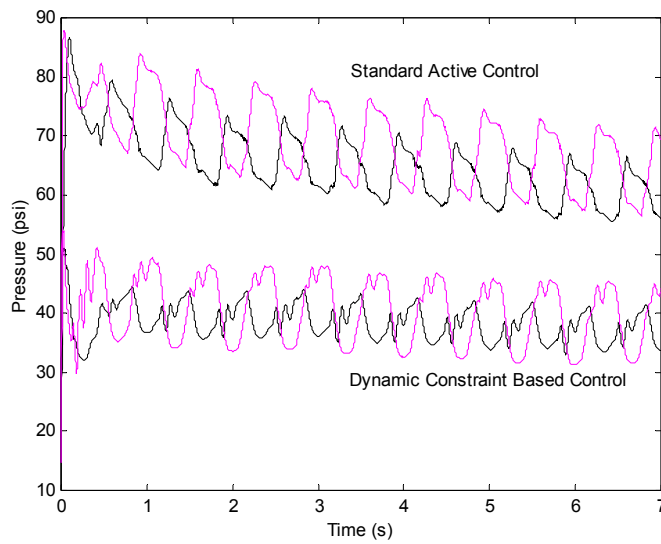


Fig. 10. Pressure variation in cylinder chambers for dynamic constraint based control versus standard sliding mode control for 1.5 Hz sinusoidal tracking (black is chamber *a* pressure, gray is chamber *b* pressure).

Frequency (Hz)	% Saving
0.25	27
0.5	45
0.75	39
1	38
1.25	36
1.5	28

Table 1. Average energy saving with dynamic constraint based control.